AD-A143 319 COMPOSITION ALTERATION OF STRATOSPHERIC AIR DUE TO SAMPLING THROUGH A FLOW TUBE(U) AIR FORCE GEOPHYSICS LAB HANSCOM AFB MA J M CALO 03 FEB 84 AFGL-TR-84-0045 1/1

UNCLASSIFIED F/G 4/1 NL

END
DATE
FILMED
8-84
DTIC

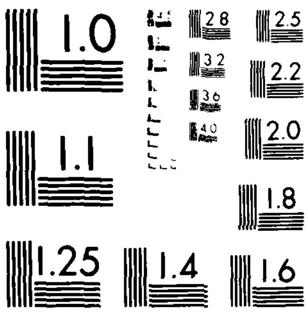

MICROCOPY RESOLUTION TEST CHART
NATIONAL BUREAU OF STANDARDS 1963-A

12

AFGL-TR-84-0045
ENVIRONMENTAL RESEARCH PAPERS, NO. [illegible]

Composition Alteration of Stratospheric Air Due to Sampling Through a Flow Tube

J.M. CALO

AD-A143 319

3 February 1984

Approved for public release; distribution unlimited.

IONOSPHERIC PHYSICS DIVISION PROJECT 4643
AIR FORCE GEOPHYSICS LABORATORY
HANSCOM AFB, MA 01731

84 07 19 025

This report has been reviewed by the ESD Public Affairs Office (PA) and is releasable to the National Technical Information Service (NTIS).

"This technical report has been reviewed and is approved for publication"

FOR THE COMMANDER

ROCCO S. NARCISI
Branch Chief

ROBERT A. SKRIVANEK, Acting Director
Ionospheric Physics Division

Qualified requestors may obtain additional copies from the Defense Technical Information Center. All others should apply to the National Technical Information Service.

If your address has changed, or if you wish to be removed from the mailing list, or if the addressee is no longer employed by your organization, please notify AFGL/DAA, Hanscom AFB, MA 01731. This will assist us in maintaining a current mailing list.

Do not return copies of this report unless contractual obligations or notices on a specific document requires that it be returned.

Unclassified

SECURITY CLASSIFICATION OF THIS PAGE (When Data Entered)

REPORT DOCUMENTATION PAGE — READ INSTRUCTIONS BEFORE COMPLETING FORM

1. REPORT NUMBER: AFGL-TR-84-0045	2. GOVT ACCESSION NO.: A143319 / 3. RECIPIENT'S CATALOG NUMBER
4. TITLE (and Subtitle): COMPOSITION ALTERATION OF STRATOSPHERIC AIR DUE TO SAMPLING THROUGH A FLOW TUBE	5. TYPE OF REPORT & PERIOD COVERED: Scientific. Interim.
	6. PERFORMING ORG. REPORT NUMBER: ERP, No. 869
7. AUTHOR(s): J.M. Calo	8. CONTRACT OR GRANT NUMBER(s)
9. PERFORMING ORGANIZATION NAME AND ADDRESS: Air Force Geophysics Laboratory (LID) Hanscom AFB Massachusetts 01731	10. PROGRAM ELEMENT, PROJECT, TASK AREA & WORK UNIT NUMBERS: 62101F 46431002
11. CONTROLLING OFFICE NAME AND ADDRESS: Air Force Geophysics Laboratory (LID) Hanscom AFB Massachusetts 01731	12. REPORT DATE: 3 February 1984
	13. NUMBER OF PAGES: 43
14. MONITORING AGENCY NAME & ADDRESS (if different from Controlling Office)	15. SECURITY CLASS. (of this report): Unclassified
	15a. DECLASSIFICATION DOWNGRADING SCHEDULE

16. DISTRIBUTION STATEMENT (of this Report)

Approved for public release; distribution unlimited.

17. DISTRIBUTION STATEMENT (of the abstract entered in Block 20, if different from Report)

18. SUPPLEMENTARY NOTES

19. KEY WORDS (Continue on reverse side if necessary and identify by block number)

Stratospheric composition
Ambient sampling

20. ABSTRACT (Continue on reverse side if necessary and identify by block number)

A numerical model of a sampling tube used to conduct stratospheric air to the sampling point of a balloon-borne cryogenic whole air sampler, has been developed to assess the potential effects of passage through the tube on alteration of species mixing ratios from those in the ambient. This model is based on the application of a general purpose, multireaction chemical kinetics code (CHEMSEN) to a 31 reaction (49 with heterogeneous wall loss), 23 species (41 with adsorbed or "lost" constituents) stratospheric kinetic model, modified to take into account heterogeneous interactions with the tube wall.

DD FORM 1 JAN 73 1473 EDITION OF 1 NOV 65 IS OBSOLETE

Unclassified

SECURITY CLASSIFICATION OF THIS PAGE (When Data Entered)

20. (Contd)

The effects of homogeneous gas phase chemistry and heterogeneous wall loss were estimated at three different altitudes: 15, 20, and 30 km. It was found that the gas phase chemistry was generally incapable of appreciably altering the sampled composition from that in the ambient. On the other hand, depending on the particular set of assumptions used, heterogeneous wall loss was found capable of imposing significant alterations on the sampled gas composition, particularly at altitudes above about 20 km, due to rapid radial diffusion. The expected tube wall temperature ~~(inferred from some related data to be well within 10 K of ambient)~~ is shown to have a negligible effect on the homogeneous gas phase kinetics in the sampling tube.

AFGL stratospheric composition data were examined in the context of possible alteration due to heterogeneous wall effects in the sampling tube. Although definitive quantitative conclusions were not possible due to the current lack of knowledge concerning the precise nature of the controlling heterogeneous phenomena and attendant rate parameter values, some qualitative hypotheses are advanced which can explain the observed trends.

The general approach presented here promises to be quite useful for the evaluation of the effects of sampling network walls on sampled gas phase compositions. However, experimental work is still needed to identify the controlling phenomena at the wall under appropriate operating conditions, and to determine accurate parameter values for use in conjunction with a numerical model such as the one presented here.

Preface

The author takes this opportunity to thank Ms. Patricia Bench for her capable and efficient work in implementing and running the numerical model, and to Ms. Pauline Beardsley for her patience in typing the manuscript. Thanks are also due to Mr. Charles C. Gallagher for providing the impetus to perform the work and for many helpful discussions along the way and in the preparation of this report.

Contents

Illustrations

Tables

Composition Alteration of Stratospheric Air Due to Sampling Through a Flow Tube

1. INTRODUCTION

Since 1974, the Air Force Geophysics Laboratory has been involved in a research program concerned with cryogenic whole air sampling of the stratosphere (see Gallagher and Pieri[1]). In this program, fixed metal cylinders (three in the most recent configurations), with specially treated inner surfaces, are immersed in a liquid helium bath surrounded by a guard volume of liquid nitrogen. This "tri whole air sampler" (TRIWAS) is the heart of the balloon flight package shown in Figure 1.

Even though this program is relatively straightforward in concept, there are many processes associated with the collection, regeneration, and analysis of complex atmospheric gas mixtures that have the potential to alter the original ambient composition of the sampled gas. The more important of these have been examined in the laboratory (for example, see Gallagher et al[2]). However, until now, not much attention has been given to the possibility of sample alteration in the relatively long intake tube extending below the gondola of the balloon, as shown in Figure 1.

(Received for publication 30 January 1984)

1. Gallagher, C.C., and Pieri, R.V. (1976) Cryogenic Whole Air Sampler and Program for Stratospheric Composition Studies, AFGL-TR-76-0162.

2. Gallagher, C.C., Forsberg, C.A., Pieri, R.V., and Faucher, G.A. (1981) Stratospheric Trace Gas Composition Studies Utilizing In Situ Cryogenic, Whole-Air Sampling Methods, AFGL-TR-81-0071, AD A104375.

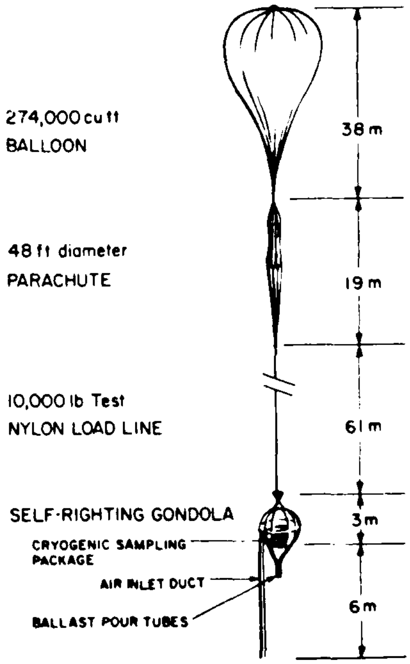

Figure 1. Balloon Flight Package for TRIWAS

Of course, once the air sample is removed from the ambient stratosphere, the photolytic mechanisms driving the in-situ steady-state chemistry cease. The resultant relaxation of reactive and semi-reactive species during their residence time in transit from the ambient atmosphere to the sampling point has the potential to modify the initial relative compositions of minor and trace species. In addition, the concentrations of reactive species and those with significant probabilities for heterogeneous removal due to adsorption reaction on the walls of the draw-in tube could be significantly reduced during their passage. The objective of this report is to assess the relative importance of sampling tube effects on the alteration of the original composition as sampled.

There is a strong resemblance between the operating characteristics of the sampling tube and those of a tubular, continuous flow chemical reactor. The current analysis makes use of this analogy in its approach to developing a diagnostic model for the sampling tube. Essentially, a general-purpose, multi-reaction chemical kinetics code (CHEMSEN) was used to describe the homogeneous gas phase kinetics, and, after suitable adaptation, heterogeneous wall effects as well. The chemical kinetics effects in the sampled air were superimposed on a fully-developed laminar flow field. The development of this approach and some sample results from the resultant model are presented in this report.

2. MODEL DEVELOPMENT

2.1 Flow Field Considerations

The Bendway® tubing that provides a constant flow of stratospheric air through the sampling point (shown in Figure 1) is about 6 m in length with an I.D. of 7.6 cm. As shown in Figure 2, at the sampling location three 2.54-cm O.D. tubes (one for each cryo-sampler volume) are located radially, 120° apart such that they terminate at the circumference of a 2.54-cm diameter circle concentric with the tube. Thus, these tubes effectively sample the central 2.54-cm diameter core of the flow in the Bendway tubing.

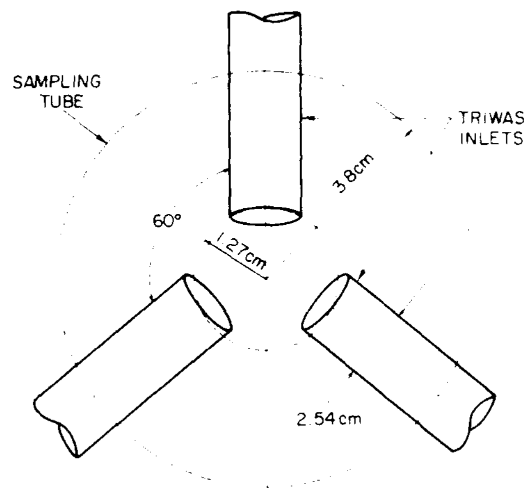

Figure 2. Schematic of the Cryogenic Sampling Point Within the Sampling Tube

Flow through the main sampling tube is maintained by an axial fan (IRW, Type VAX-2MM Vaneaxial blower) rated at 40 CFM, located downstream of the sampling point. Flight data with the same type of fan in another program (see Sherman[3]) indicates that the volumetric displacement of this fan remains relatively constant

3. Sherman, C. (1983) private communication.

at the rated value until about 30 km, where a reduction in capacity of approximately one-third is indicated. Thus, at rated capacity, the volumetric flowrate should be about 1.89×10^4 cm^3/sec, which in the 30 km region drops to about 1.26×10^4 cm^3/sec. Using these figures and a cross sectional area of 45.4 cm^2, the average velocity in the sampling tubing is:

$$\bar{u} = q/A = 416 \text{ cm/sec } (277.5 \text{ cm/sec at 30 km}) .$$

Assuming typical stratospheric conditions (U.S. Standard Atmosphere[4]):

15 km: 216.65K; 90.85 torr; 4.05×10^{18} cm^{-3}
20 km: 216.67K; 41.47 torr; 1.8×10^{18} cm^{-3}
30 km: 231.24K; 8.99 torr; 3.7×10^{17} cm^{-3} .

The viscosity of air at these conditions (from Bird et al,[5] pp. 16-17) is $\mu \simeq 0.015$ c_p. Thus, the corresponding Reynolds numbers are:

$$Re = D\bar{u}\rho/\mu$$
$$Re\ (15\text{ km}) = 4110$$
$$Re\ (20\text{ km}) = 1827$$
$$Re\ (30\text{ km}) = 250 .$$

Thus, even though the Reynolds number at 15 km is in the transitional flow regime, under most sampling conditions the fully developed flow field in the tube should be laminar; that is, $Re < 2100$.

Taking the preceding into consideration, the conditions in the sampled central core ($-R_1 < r < R_1$) will be characterized by an average velocity, $\bar{u}R_1$, and an average concentration, C_{m, R_1}. Averaging over the familiar parabolic flow velocity profile:

$$\bar{u}_{R_1} = \frac{\int_0^{R_1} u_o \left(1 - r^2/R^2\right) rdr}{\int_0^{R_1} rdr} \tag{1}$$

---

4. U.S. Standard Atmosphere (1976) NOAA, NASA, USAF, Washington, D.C.
5. Bird, R.B., Stewart, W.E., and Lightfoot, E.H. (1960) Transport Phenomena, Wiley & Sons, New York.

$$\bar{u}_{R_1} = u_o \left[1 - \frac{R_1^2}{2\,R^2} \right] . \qquad (2)$$

For the current situation, $R_1 = 1.27$ cm and $R = 3.8$ cm, and thus,

$$\bar{u}_{R_1} = u_o \left[1 - \frac{(1.27)^2}{2(3.8)^2} \right] = 0.944\, u_o \qquad (3)$$

or

$$\bar{u}_{R_1} = 0.944\,(2\bar{u}) = 0.944\,(2 \times 416) = 785 \text{ cm/sec } (524 \text{ cm/sec at } 30 \text{ km}) .$$

Thus, the central core travels at a mean velocity of 785 cm/sec. The mean core concentration is estimated in Section 2.3.

2.2 Axial Convection vs Radial Diffusion

In order to assess the potential importance of diffusional losses to the tube wall, the relative time scales of axial convection and radial diffusion must be compared. The general problem of dispersion in laminar tube flow has received considerable attention in the literature; the classic analysis of Taylor[6,7,8] having been amplified on numerous occasions (for example, see Aris[9] and Hunt[10]). Referring to Taylor[6] the characteristic time for convection through the sampling tube is given by:

$$\tau_{conv.} = L/u_o , \qquad (4)$$

where L is the sampling tube length (6 m); while that for radial diffusion is given by:

$$\tau_{diff} = (R/3.8)^2/D , \qquad (5)$$

where D is the molecular diffusivity and R is the tube radius (3.8 cm). A comparison of these time scales at three altitudes for NO in air yields:

(Due to the large number of references cited above, they will not be listed here. See References, page 39.)

Altitude (km)	$D(NO_2)$ (cm^2/sec)	$\tau_{conv.}$ (s)	$\tau_{diff.}$ (s)
15	1.	0.72	1.0
20	2.	0.72	0.5
30	10.	1.08	0.1

where the molecular diffusivities were estimated from Bird et al[5] [Eq. (16.3-1), p. 505]. Thus, at low altitudes $\tau_{conv.}$ and $\tau_{diff.}$ are of comparable magnitude. However, with increasing altitude $\tau_{diff.} < \tau_{conv.}$, due to the proportional increase in D with decreasing pressure (that is, $D \propto 1/P$). For purposes of estimating the possible magnitude of heterogeneous wall effects on alteration of the composition of the sampled air, only cases where $\tau_{diff.} < \tau_{conv.}$ will be of interest. However, as the preceding calculation shows, this situation prevails for a significant range of stratospheric altitudes over which sampling has been carried out.

For conditions where $\tau_{diff.} < \tau_{conv.}$, a *method* was developed for estimating the magnitude of heterogeneous wall effects. This approach is based upon the fact that under these conditions, the radial concentration profile due to diffusion is rapidly established. A species mass balance for this situation results in the familiar Bessel function solution for cylindrical geometry (for example, see Crank,[11] p. 72):

$$C(z,t) = \sum_{n=1}^{\infty} A_n J_o(\alpha_n^{1/2} D^{-1/2} Rz) \exp(-\alpha_n t) \tag{6}$$

where J_o is the zeroth order Bessel function of the first kind, the α_n are constants determined by the boundary conditions, A_n are constants determined by application of orthogonality of the Bessel functions, t is time, and $z = r/R$.

2.3 Heterogeneous Wall Loss Estimation Technique

In order to use the multireaction chemical kinetic code, CHEMKIN (Kee et al[12]) to model the homogeneous reaction behavior in the sampling tube, and also to estimate the effects of wall termination, the heterogeneous loss due to radial diffusion *must be estimated* and transformed into an approximate pseudo-homogeneous reaction. The development of the resultant averaging technique follows.

---

11. Crank, J. (1975) The Mathematics of Diffusion, Oxford University Press, London.
12. Kee, R.J., Miller, J.A., and Jefferson, T.H. (1980) CHEMKIN: A General-Purpose, Problem-Independent, Transportable, FORTRAN Chemical Kinetics Code Package, SAND 80-8003, Sandia National Laboratories, Livermore, California.

At the tube wall ($r = R$, or $z = 1$), a steady-state mass balance yields:

$$-D \left. \frac{\partial C}{\partial r} \right|_{r=R} = k\, C_{r-R} \tag{7}$$

where k is the heterogeneous loss rate constant (cm/sec). Making use of Eq. (6):

$$\left. \frac{\partial C}{\partial r} \right|_{r=R} = \left(\frac{1}{R}\right) \left. -\frac{\partial C}{\partial z} \right|_{z=1} \tag{8}$$

$$= -\sum_{n=1}^{\infty} A_n \alpha_n^{1/2} D^{-1/2} J_1(\alpha_n^{1/2} D^{-1/2} R) \exp(-\alpha_n t)$$

where J_1 is the first order Bessel function of the first kind. Substituting this expression into Eq. (7):

$$\sum_{n=1}^{\infty} A_n D^{1/2} \alpha^{1/2} J_1(\alpha^{1/2} D^{-1/2} R) \exp(-\alpha_n t)$$

$$= k \sum_{n=1}^{\infty} A_n J_o(\alpha_n^{1/2} D^{-1/2} R) \exp(-\alpha_n t) \,. \tag{9}$$

Approximating both sides of Eq. (9) by the first term in the series, (which becomes a better approximation as time progresses):

$$\alpha_1 = \frac{k^2}{D} \left[\frac{J_o(\alpha_1^{1/2} D^{-1/2} R)}{J_1(\alpha_1^{1/2} D^{-1/2} R)} \right]^2 \,. \tag{10}$$

The effective loss rate for a particular species in the central sampled core, $-R_1 \leq r \leq R_1$ ($R_1 = 1.27$ cm), due to steady-state wall termination is given by:

$$-D \left. \frac{\partial C}{\partial r} \right|_{r=R_1} \frac{\pi R_1^2}{2\pi R_1} k' C_{m, R_1} \tag{11}$$

where k' is a pseudo-homogeneous first order rate constant (sec^{-1}), and C_{m, R_1} is the mean concentration in the sampled central core. Eq. (11) effectively transforms the diffusive loss rate at the boundary of the sampled central core to an approximate, pseudo-homogeneous loss rate based upon the mean concentration in the core.

The mean concentration, C_{m, R_1} is determined by averaging the concentration profile over r:

$$C_{m,R_1} = \frac{\int_0^{R_1} C(r)\, r\, dr}{\int_0^{R_1} r\, dr} \tag{12}$$

or, substituting Eq. (6) for $C(r)$:

$$C_{m,R_1} = 2\int_0^{R_1} \frac{\sum_{n=1}^{\infty} A_n J_o(\alpha_n^{1/2} D^{-1/2} r) \exp(-\alpha_n t)\, r dr}{R_1^2} \, . \tag{13}$$

Solution of Eq. (13), once again using the first term approximation, yields:

$$C_{m,R_1} = 2\left(\frac{R}{R_1}\right) A_1 \frac{J_1(\alpha_1^{1/2} D^{-1/2} R_1) \exp(-\alpha_n t)}{\alpha_1^{1/2} D^{-1/2} R} \, . \tag{14}$$

Substitution of Eq. (14) into Eq. (11) yields:

$$k' = \alpha_1 \, . \tag{15}$$

For instantaneous loss at the wall ($r = R$),

$$C_{r=R} = 0 = \sum_{n=1}^{\infty} A_n J_o(\alpha_n^{1/2} D^{-1/2} R) \exp(-\alpha_n t) \tag{16}$$

or, using the first term and first root of J_o,

$$\alpha_1^{1/2} D^{-1/2} R = 2.4 \tag{17}$$

Substituting into Eq. (15)

$$k' = (2.4)^2 D / R^2 \tag{18}$$

which is the approximate representation of the upper limit, pseudo-homogeneous, first order rate constant for heterogeneous wall loss.

The rate constants representing wall loss can also be interpreted in terms of a fractional loss of the upper limit value given by Eq. (18). For complete wall destruction:

$$N(\text{wall flux}) = -D \left.\frac{\partial C}{\partial r}\right|_{r=R}$$

$$= \frac{D}{R} \sum_{n=1}^{\infty} A_n (\alpha_n^{1/2} D^{-1/2} R)\, J_1(\alpha^{1/2} D^{-1/2} R) \exp(-\alpha_n t) \,. \qquad (19)$$

Substituting for α_1, using Eq. (17), and the first term in the summation:

$$N = D\, C_o\, 2.4\; J_1(2.4)/R$$

or

$$N = D\, C_o\, 1.25/R \,, \qquad (20)$$

which represent the upper limit wall flux for complete destruction. If, f is the fractional destruction at the wall, then combination of Eqs. (7) and (16) with the definition of f yields:

$$f = \frac{k\, C_o\, J_o(\alpha_1^{1/2} D^{-1/2} R)}{D\, C_o\, 1.25 / R} \qquad (21)$$

or, upon rearrangement:

$$k = f\, D\, 1.25/R\, J_o(\alpha_1^{1/2} D^{-1/2} R) \,. \qquad (22)$$

Elimination of k between Eqs. (10) and (22) results in:

$$\alpha_1^{1/2} = \frac{f\, D^{1/2}\, 1.25}{R\, J_1(\alpha_1^{1/2} D^{-1/2} R)} \,. \qquad (23)$$

Thus, specification of f, along with the parameters D and R, defines α_1 via solution of Eq. (23). However, Eq. (23) is transcendental in α_1 and thus requires an iterative solution. An appropriate iterative solution scheme using Newton's method is formulated in Appendix A. Of course, once α_1 is determined, then k' follows directly from Eq. (15); namely, $k' = \alpha_1$. A plot of the heterogeneous wall loss rate constant in dimensionless form $(k' R^2/D)$ as a function of f is presented in Figure 3.

The corresponding rate constant values for specified f are:

f	k'
0	0
$0 < f < 1$	Eq. (23), $k' = \alpha_1$
$f = 1$	$(2.4)^2 D/R^2$

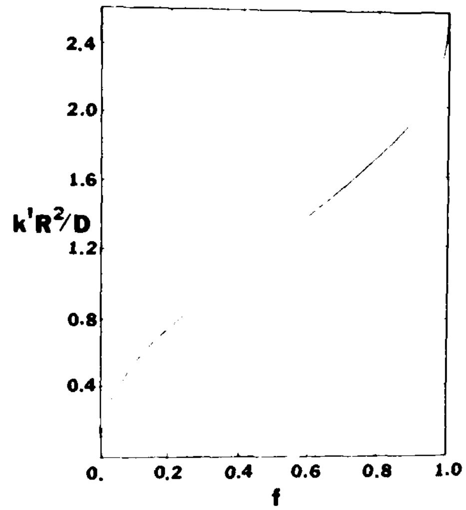

Figure 3. Dimensionless Heterogeneous Rate Constant as a Function of Fraction of the Maximum Wall Loss Rate

3. COMPUTATIONAL CODE

The entire preceding development was undertaken with the objective of adapting an existing code based on CHEMKIN (Kee et al[12]), to calculate composition changes along the sampling tube due to chemical reactions. The particular version of this code available was intended primarily for the solution of homogeneous kinetic problems without transport. Thus, the method in Section 2.3 was formulated in order to transform the wall termination reactions into equivalent "pseudo-homogeneous" form.

3.1 CHEMKIN et al

CHEMKIN is a package of FORTRAN programs designed to facilitate general chemical kinetic modeling of multireaction, multispecies problems. It was developed at Sandia National Laboratories, Livermore by Kee and associates (Kee et al[12]). Essentially, it accepts the definition of a chemical kinetic mechanism in familiar,

relatively "format-free" chemical notation, and transforms it into FORTRAN code, *which can then be manipulated in almost any manner the user chooses.* For the current applications, CHEMKIN was used in combination with a general ordinary differential equation solver, LSODE, and appropriate subroutines to transform the FORTRAN code from CHEMKIN into the corresponding mass conservation equations for solution by LSODE. This particular combination was available as SENSIT, a sensitivity code package developed by Kramer et al.,[13] that features the powerful new AIM (analytically integrated Magnus) modification of the GFM (Green's function method) for sensitivity analysis of ODE systems.

3.2 Chemical Kinetic Mechanism

The chemical kinetic mechanism formulated for use with the CHEMKIN SENSIT code package was, of course, essentially a basic stratospheric chemical kinetic model <u>sans</u> the photolytic formation and destruction reactions. The actual mechanism used was extracted primarily from "The Stratosphere 1981...",[14] along with the corresponding rate constants in appropriate form and units for use in the CHEMKIN SENSIT code. This mechanism is presented in Table 1, along with the corresponding rate parameters.

In order to model heterogeneous wall termination reactions, most of the species were provided with a reaction of the form:

$$S \rightarrow S( ) .$$

The pseudo-homogeneous rate constants, k , for these reactions were estimated according to the method presented in Section 2.3. The specification that appears in the mechanism definition input next to the ( ) reactions is the negative of f, the fraction of the total wall destruction rate assumed for that species. Using -f as the input, the subroutine KPRIME (listed in Appendix B) returns the pseudo-homogeneous first order rate constant, k', for use in the model.

---

13. Kramer, M.A., Kee, R.J., and Rabitz, H. (1982) <u>CHEMSEN: A Computer Code for Sensitivity Analysis of Elementary Chemical Reaction Models, SAND 82-8230</u>, Sandia National Laboratories, Livermore, California.
14. <u>The Stratosphere, 1981, Theory and Measurements</u> (1982) WMO, NASA, FAA, NOAA, Report No. 11, NASA/Goddard Space Flight Center, Greenbelt, Maryland.

Table 1. Stratospheric Kinetic Model[a]

(A) Bimolecular Reactions

No.	Reaction	k_2: $\underline{A}_o$[b] ($\mathrm{s\ mol/cm^3})^{-1}$	k_2: $\underline{E}$[b] (cal/mol)
1.	$O + O_3 \rightarrow 2O_2$	0.900E + 13	4407.
2.	$NO_2 + O \rightarrow NO + O_2$	0.560E + 13	0.
3.	$O_3 + NO \rightarrow NO_2 + O_2$	0.230E + 13	3150.
4.	$NO + ClO \rightarrow NO_2 + Cl$	0.370E + 13	-584.
5.	$NO + HO_2 \rightarrow NO_2 + HO$	0.220E + 13	-477.
6.	$NO_2 + O_3 \rightarrow NO_3 + O_2$	0.720E + 11	4868.
7.	$NO_3 + NO \rightarrow 2\,NO_2$	0.120E + 14	0.
8.	$HNO_4 + HO \rightarrow NO_2 + H_2O + O_2$	0.240E + 13	0.
9.	$HNO_3 + HO \rightarrow NO_3 + H_2O$	0.900E + 10	-1292.
10.	$HO_2 + HO \rightarrow H_2O + O_2$	0.480E + 14	0.
11.	$HO_2 + HO_2 \rightarrow H_2O_2 + O_2$	0.180E + 13	0.
12.	$HO_2 + O \rightarrow HO + O_2$	0.210E + 14	0.
13.	$HO_2 + ClO \rightarrow HOCl + O_2$	0.290E + 14	0.
14.	$HO_2 + O_3 \rightarrow HO + 2O_2$	0.840E + 10	1152.
15.	$HO + O_3 \rightarrow HO_2 + O_2$	0.960E + 12	1868.
16.	$HO + O \rightarrow H + O_2$	0.140E + 14	-219.
17.	$HO + CO \rightarrow H + CO_2$	0.810E + 11	0.
18.	$HO + H_2 \rightarrow H + H_2O$	0.460E + 13	4173
19.	$H_2O_2 + HO \rightarrow H_2O + HO_2$	0.160E + 13	288.
20.	$Cl + O_3 \rightarrow ClO + O_2$	0.170E + 14	511.
21.	$ClO + O \rightarrow Cl + O_2$	0.460E + 14	258.
22.	$N_2O_5 + M \rightarrow NO_2 + NO_3 + M$	0.140E + 00	0.
23.	$Cl + H_2 \rightarrow H + HCl$	0.211E + 14	4550.
24.	$HO_2 + Cl \rightarrow O_2 + HCl$	0.289E + 13	0.

Table 1. Stratospheric Kinetic Model[a] (Contd)

(B) Termolecular Reactions

No.	Reaction	k_3: A_o[c] $\left[s\,(mol/cm^3)^2\right]^{-1}$	β
25.	$O + O_2 + M \rightarrow O_3 + M$	0.200E+20	-2.0
26.	$NO_2 + O + M \rightarrow NO_3 + M$	0.390E+21	-2.0
27.	$NO_2 + HO + M \rightarrow HNO_3 + M$	0.530E+25	-2.9
28.	$NO_2 + HO_2 + M \rightarrow HNO_4 + M$	0.580E+29	-5.0
29.	$NO_3 + NO_2 + M \rightarrow N_2O_5 + M$	0.160E+24	-2.8
30.	$H + O_2 + M \rightarrow HO_2 + M$	0.590E+20	-1.4
31	$ClO + NO_2 + M \rightarrow ClONO_2 + M$	0.460E+18	-1.9

(C) Heterogeneous Reactions

No.	Reaction
32.	$NO \rightarrow NO$ (*)
33.	$NO_2 \rightarrow NO_2$ ( )
34.	$N_2O_5 \rightarrow N_2O_5$ ( )
35.	$NO_3 \rightarrow NO_3$ ( )
36.	$HNO_3 \rightarrow HNO_3$ ( )
37.	$HNO_4 \rightarrow HNO_4$ ( )
38.	$O \rightarrow O$ ( )
39.	$O_3 \rightarrow O_3$ ( )
40.	$HO \rightarrow HO$ ( )
41.	$HO_2 \rightarrow HO_2$ ( )
42.	$H_2O_2 \rightarrow H_2O_2$ ( )
43.	$Cl \rightarrow Cl$ ( )
44.	$ClO \rightarrow ClO$ ( )
45.	$H \rightarrow H$ ( )
46.	$HOCl \rightarrow HOCl$ ( )
47.	$H_2O \rightarrow H_2O$ ( )
48.	$ClONO_2 \rightarrow ClONO_2$ (*)
49.	$HCl \rightarrow HCl$ ( )

(a) The Stratosphere 1981...,[14] Tables A1 and A2.

(b) $k_2 = A_o \exp(-E/RT)$, $(s\ mol/cm^3)^{-1}$ (Table A1)

(c) $k_3 = A_o T^{\beta}$, $\left[s\,(mol/cm^3)^2\right]^{-1}$ (Table A2)

4. RESULTS AND DISCUSSION

4.1 Cases and Data

Three different altitudes, spanning the range of the stratospheric whole-air sampling program, were considered; namely, 15, 20, and 30 km. The initial concentrations for most of the species were obtained from the Stratosphere 1981...[14] and Fabian et al.[15] Two sets of NO and NO_2 values were used: averages of all the mid-latitude AFGL data, and those of Fabian et al.[15] Summaries of all values used are presented in Table 2.

The final "f" values used for the heterogeneous wall termination reactions were much more difficult to assign. Of course, values of f= 1 are probably quite appropriate for all the free radical species. However, the precise degree of interaction of semireactive and stable species with the walls of the sampling tube is, for the most part, unknown. Ultimately, "f" values for these species were varied in order to assess their effect.

Characterization of the controlling processes of all the various heterogeneous phenomena that can occur at the walls of the sampling tube remains an important unresolved issue. As shown below, these heterogeneous processes have at least the potential to alter both the relative and absolute concentrations of the NO_x HNO_x species from those in the ambient. The following discussion is intended to highlight some of the potentially more important processes that may occur.

First of all, conditions at the sampling tube wall were assumed to be at steady-state when a sample is taken. This assumption is quite reasonable in view of the fact that air was continuously drawn through the sampling tube, once at altitude, for at least a half hour prior to the cryogenic sample actually being taken. Thus, at the ambient temperatures expected (see Section 4.3), the tube wall is most probably coated with a layer of condensed water.

NO_2 is known to be rapidly converted to NO by reaction with adsorbed water (Greene and Past[16]). The requisite stoichiometry is believed to be:

$$2NO_2 + H_2O \rightarrow HNO_2 + HNO_3 . \qquad (24)$$

---

15. Fabian, P., Pyle, J.A., and Wells, R.J. (1982) Diurnal variations of minor constituents in the stratosphere modeled as a function of latitude and season, J. Geophys. Res. 87:4981.

16. Greene, S.A., and Pust, H. (1958) Determination of nitrogen dioxide by gas-solid chromatography, Anal. Chem. 30:1039.

Table 2. Initial Species Concentration

Species	Source	Concentration (mol fraction) 15 km	20 km	30 km
NO	(c, d)	1.5E-09	2.4E-09	5.7E-09
NO_2	(c, d)	2.1E-09	4.3E-09	10.8E-09
NO_3	(a)	4.0E-15	2.0E-14	4.0E-13
HNO_3	(a)	1.3E-09	6.0E-09	6.0E-09
HNO_4	(b)	7.6E-11	4.8E-10	1.9E-10
N_2O_5	(a)	2.0E-12	1.3E-11	1.3E-10
O	(b)	5.7E-14	1.1E-12	2.2E-10
O_2	-	0.209	0.209	0.209
N_2	-	0.79067	0.79067	0.79066
O_3	(a)	5.0E-07	2.2E-06	1.6E-05
HO	(a)	8.0E-11	2.0E-12	7.0E-11
HO_2	(a)	1.1E-11	1.2E-11	1.5E-10
H_2O_2	(a)	1.5E-09	2.0E-09	6.0E-09
H_2O	-	3.0E-06	3.0E-06	3.0E-06
Cl	(a)	1.0E-15	6.0E-15	7.0E-12
ClO	(a)	1.5E-12	3.0E-11	1.5E-10
H	(b)	3.5E-17	3.5E-17	3.5E-7
HOCl	(b)	1.0E-10	1.0E-10	1.0E-10
CO	(b)	1.0E-08	1.0E-08	1.0E-08
CO_2	-	3.2E-04	3.2E-04	3.2E-04
H_2	(b)	5.0E-06	5.0E-06	5.0E-06
$ClONO_2$	(b)	5.0E-12	2.0E-10	5.0E-10
HCl	(b)	4.0E-11	1.0E-10	2.0E-10

(a) The Stratosphere 1981, Theory and Measurements, WMO, NASA, FAA, NOAA, Report No. 11, May 1981, NASA/Goddard Space Flight Center, Greenbelt, Maryland.[14]

(b) Fabian et al.[15]

(c) AFGL data.

(d) The corresponding values from Reference (b) are:
15 km, NO = 4.0E-11, NO_2 = 4.0E-11;
20 km, NO = 1.0 x E-10, NO_2 = 3.0E-10;
30 km, NO = 1.0 x E-09, NO_2 = 5.0E-09.

Under conditions where nitrous acid is unstable (that is, at room temperature and above), it would decompose according to the stoichiometry:

$$3HNO_2 \rightarrow HNO_3 + 2NO + H_2O. \quad (25)$$

The net effect of [R1] and [R2] is:

$$3NO_2 + H_2O \rightarrow 2HNO_3 + NO \quad (26)$$

or one NO for every $3NO_2$ consumed. If this process is important at stratospheric conditions on the sampling tube walls, obviously the NO/NO_x *ratio* at the final sampling point would be significantly larger than the ambient value at altitudes where there is rapid diffusion to the walls (for example, 30 km). Actually, however, this possibility is quite unlikely. The conditions under which Greene and Pust[16] observed this conversion process involved a chromatographic column packed with Linde 5A molecular sieve saturated with water, and with NO_2 near atmospheric pressure. At the operating temperatures of the sampling tube in the stratosphere, any nitrous and/or nitric acid formed on the tube walls would remain there in the condensed water matrix. Thus, although NO_2 most probably adsorbs/reacts on the tube wall with a large capture coefficient, *the decomposition of nitrous acid* [illegible] (25) should not occur to any appreciable extent, thereby preventing the release of product NO back into the gas phase. In summary then, primarily due to expected temperatures at the tube wall, the most conservative assumption would be that all the NO_x/HNO_x species (except NO) that reach the wall are lost from the gas phase with a capture coefficient of unity.

Nitric oxide is normally a noncondensable gas. True thermodynamic condensation of any species occurs when the pressure exerted by the incident flux of that species equals the vapor pressure of the condensed phase; although in most actual situations some supersaturation due to heterogeneous nucleation is observed (for example, see Bentley and Hands[17]). For the ambient levels of NO [illegible] 30 km, the highest possible wall flux in the sampling tube at the inlet is only [illegible] 3×10^{14} [illegible]$^{-2}$ sec^{-1}. Under these conditions, pure NO would be expected to condense at or below [illegible] 30 K. Thus, obviously, pure NO should not condense on the sampling tube walls due to normal condensation. However, in an experimental study of cryogenic condensation of atmospheric gases (Calo et al[18]), NO was found to be [illegible]

---

17. Bentley, P.D., and Hands, B.A. [illegible] Proc. Roy. Soc. London [illegible]

18. Calo, J.M., Fezza, R.J., and Dineen, E.J. [illegible] Gas-Surface Interactions in Cryogenic Whole Air Sampling, AFGL-TR-81-0162, AD A10[illegible].

efficiently trapped by condensed water (most probably as mixed clathrate hydrates) at relatively high temperatures, exactly in the range expected for the sampling tube walls (that is, 216 to 230 K). Rather than being true thermodynamic condensation, this phenomenon is a complex kinetic entrapment process favored by high fluxes of both the species and water vapor. In the case of the sampling tube, however, even though the temperatures at altitude are in the requisite range, the fluxes seem to be too low for this effect to be important; that is, $10^{19} - 10^{20}$ m^{-2} sec^{-1} for both NO and H_2O in the experiments cited, vs $\sim 3 \times 10^{14}$ and $\sim 2 \times 10^{17}$ m^{-2} sec^{-1}, respectively, at the conditions in the sampling tube case. Based on these considerations, it is judged that NO is most probably not removed to any significant extent at the sampling tube walls; that is, $f = 0$, would be a reasonable assumption.

Although the preceding discussion is intended to focus on the most likely first order effects expected to occur at the tube wall, it is, perhaps, more realistic to think of the behavior of the tube at high altitudes where radial diffusivities are large, as approximating that of a chromatographic column. The interactions among the various species and the condensed phase on the tube wall can be quite complex and nonlinear, and thus, almost impossible to estimate a priori. Currently, the only manner in which to obtain realistic "f" values for the various species under sampling conditions and concentrations is experimentally.

4.2 Model Results

4.2.1 GENERAL

Some model results for various cases of heterogeneous wall loss are presented in Table 3 [(a), (b), and (c) for 15, 20, and 30 km, respectively], in terms of fractions of initial ambient concentrations at the final cryogenic sampling point. The conditions for the various cases are included in the legend for Table 3. The same results are presented in Table 4 [(a), (b), and (c)] in terms of three NO/NO_x ratios. The cases in both Tables 3 and 4 are the same.

Table 3. Ratios of Species Concentrations at the Sampling Point to the Ambient, (a) 15 km, (b) 20 km, and (c) 30 km

Legend

Case I.	$f = 0$ for species		
Case II.	$f = 1$ for all species except CO, CO_2, O_2, N_2 and H_2 ($f = 0$).		
Case III.	$f = 0.5$ for all species except CO, CO_2, O_2, N_2 and H_2 ($f = 0$).		
Case IV.	$f = 1$ for all species except NO, CO, CO_2, O_2, N_2 and H_2 ($f = 0$).		
The following four cases are similar to the preceding except that NO and NO_2 values are taken from Fabian et al.[15]			
Case V.	Equivalent to Case I.	Case VII.	Equivalent to Case III.
Case VI.	Equivalent to Case II.	Case VIII.	Equivalent to Case IV.

Table 3. Ratios of Species Concentrations at the Sampling Point to the Ambient, (a) 15 km, (b) 20 km, and (c) 30 km (Contd)

Species / Case	(a) 15 km I	II	III	IV	V	VI	VII	VIII
NO	0.995	0.737	0.919	0.996	0.996	0.736	0.919	0.996
NO_2	1.001	0.836	0.931	0.761	1.004	0.762	0.934	0.763
NO_3	23.775	12.535	21.315	15.635	16.152	16.000	21.790	15.998
HNO_3	1.004	0.845	0.937	0.773	1.000	0.771	0.934	0.771
HNO_4	1.000	0.848	0.936	0.778	0.999	0.778	0.935	0.777
N_2O_5	1.000	0.854	0.938	0.785	1.000	0.785	0.938	0.785
CO	1.000	1.000	1.000	1.000	1.000	1.000	1.000	1.000
CO_2	1.000	1.000	1.000	1.000	1.000	1.000	1.000	1.000
O	~0.	~0.	~0.	~0.	~0.	~0.	~0.	~0.
O_2	1.000	1.000	1.000	1.000	1.000	1.000	1.000	1.000
O_3	1.000	0.837	0.931	0.761	1.000	0.761	0.931	0.761
HO	0.896	0.742	0.818	0.637	0.964	0.668	0.863	0.668
HO_2	1.252	0.955	1.151	0.907	1.216	0.959	1.216	0.959
H_2O_2	1.000	0.825	0.925	0.746	1.000	0.746	0.892	0.746
H_2O	1.000	0.797	0.912	0.706	1.000	0.706	0.579	0.706
N_2	1.000	1.000	1.000	1.000	1.000	1.000	1.000	1.000
$ClONO_2$	1.000	0.852	0.937	0.783	1.000	0.783	0.937	0.783
HCl	1.000	0.828	0.927	0.750	1.000	0.750	0.927	0.750
Cl	12.280	10.130	11.350	11.960	0.324	0.245	0.305	0.322
ClO	0.991	0.831	0.923	0.755	0.999	0.763	0.930	0.508
H	0.103	0.084	0.094	0.073	0.111	0.077	0.099	0.077
HOCl	1.000	0.839	0.932	0.765	1.000	0.839	0.932	0.765
H_2	1.000	1.000	1.000	1.000	1.000	1.000	1.000	1.000

Table 3. Ratios of Species Concentrations at the Sampling Point to the Ambient, (a) 15 km, (b) 20 km, and (c) 30 km (Contd)

Species / Case	(b) 20 km I	II	III	IV	V	VI	VII	VIII
NO	0.991	0.517	0.834	0.993	0.994	0.517	0.834	0.993
NO_2	1.005	0.554	0.859	0.555	1.002	0.553	0.857	0.554
NO_3	2.156	1.056	1.7785	1.041	1.2075	0.697	1.109	0.696
HNO_3	1.000	0.570	0.862	0.570	1.000	0.570	0.862	0.570
HNO_4	1.000	0.580	0.866	0.580	1.000	0.580	0.866	0.580
N_2O_5	1.000	0.592	0.871	0.592	1.000	0.592	0.866	0.592
CO	1.000	1.000	1.000	1.000	1.000	1.000	1.000	1.000
CO_2	1.000	1.000	1.000	1.000	1.000	1.000	1.000	1.000
O	~0.	~0.	~0.	~0.	~0.	~0.	~0.	~0.
O_2	1.000	1.000	1.000	1.000	1.000	1.000	1.000	1.000
O_3	1.000	0.554	0.856	0.554	1.000	0.554	0.856	0.554
HO	1.124	0.512	0.912	0.540	0.965	0.446	0.776	0.447
HO_2	0.968	0.515	0.819	0.510	1.003	0.530	0.848	0.530
H_2O_2	1.000	-.530	0.846	0.530	1.000	0.530	0.846	0.530
H_2O	1.000	0.471	0.820	0.471	1.000	0.471	0.820	0.471
N_2	1.000	1.000	1.000	1.000	1.000	1.000	1.000	1.000
$ClONO_2$	1.000	0.588	0.869	0.588	1.000	0.588	0.869	0.588
HCl	1.000	-.536	0.848	0.536	1.000	0.536	0.848	0.536
Cl	14.907	7.845	12.582	14.430	0.622	0.328	0.526	0.604
ClO	0.996	0.557	0.854	0.555	1.000	0.558	0.857	0.558
H	0.007	0.003	0.006	0.004	0.006	0.003	0.005	0.003
HOCl	1.000	0.560	0.858	0.560	1.000	0.560	0.858	0.560
H_2	1.000	1.000	1.000	1.000	1.000	1.000	1.000	1.000

Table 3. Ratios of Species Concentrations at the Sampling Point to the Ambient, (a) 15 km, (b) 20 km, and (c) 30 km (Contd)

Species / Case	(c) 30 km I	II	III	IV	V	VI	VII	VIII
NO	0.981	0.012	0.259	0.995	0.981	0.006	0.259	0.996
NO_2	1.010	0.018	0.346	0.010	1.004	0.010	0.296	0.010
NO_3	1.338	0.023	0.429	0.013	1.117	0.013	0.349	0.013
HNO_3	1.000	0.022	0.365	0.013	1.000	0.013	0.316	0.013
HNO_4	1.000	0.025	0.377	0.015	1.000	0.015	0.327	0.015
N_2O_5	1.000	0.028	0.391	0.017	1.000	0.017	0.341	0.017
CO	1.000	1.000	1.000	1.000	1.000	1.000	1.000	1.000
CO_2	1.000	1.000	1.000	1.000	1.000	1.000	1.000	1.000
O	~0.	~0.	~0.	~0.	~0.	~0.	~0.	~0.
O_2	1.000	1.000	1.000	1.000	1.000	1.000	1.000	1.000
O_3	1.000	0.018	0.348	0.010	1.000	0.012	0.298	0.010
HO	1.015	0.006	0.259	0.003	0.931	0.002	0.199	0.003
HO_2	0.991	0.013	0.317	0.007	1.008	0.007	0.271	0.007
H_2O_2	1.000	0.014	0.321	0.007	1.000	0.007	0.273	0.007
H_2O	1.000	0.006	0.260	0.003	1.000	0.003	0.214	0.003
N_2	1.000	1.000	1.000	1.000	1.000	1.000	1.000	1.000
$ClONO_2$	1.000	0.027	0.387	0.016	1.000	0.016	0.337	0.016
HCl	1.000	0.014	0.327	0.008	1.000	0.008	0.278	0.008
Cl	0.030	~0.	0.009	0.005	0.005	~0	0.002	0.010
ClO	1.042	0.020	0.368	0.011	1.043	0.014	0.316	0.011
H	0.806	0.004	0.204	0.004	0.734	0.002	0.156	0.002
HOCl	1.005	0.020	0.355	0.011	1.004	0.011	0.305	0.011
H_2	1.000	1.000	1.000	1.000	1.000	1.000	1.000	1.000

Table 4. NO/NO_x for the Eight Computational Cases in Table 3, (a) 15 km, (b) 20 km, and (c) 30 km

(a) 15 km

Ratio	Ambient	I	II	III	IV
NO/NO_x [a]	0.417	0.300	0.274	0.298	0.359
$NO/(NO + NO_2)$	0.417	0.415	0.386	0.414	0.483
NO/NO_2	0.714	0.710	0.630	0.705	0.935
	Ambient	V	VI	VII	VIII
NO/NO_x [a]	0.027	0.027	0.026	0.027	0.035
$NO/(NO + NO_2)$	0.500	0.498	0.491	0.496	0.566
NO/NO_2	1.000	0.992	0.966	0.984	1.305

(b) 20 km

Ratio	Ambient	I	II	III	IV
NO/NO_x [a]	0.181	0.180	0.169	0.177	0.281
$NO/(NO + NO_2)$	0.358	0.355	0.342	0.351	0.500
NO/NO_2	0.558	0.550	0.521	0.542	0.999
	Ambient	V	VI	VII	VIII
NO/NO_x [a]	0.014	0.014	0.013	0.014	0.0250
$NO/(NO + NO_2)$	0.250	0.248	0.238	0.245	0.374
NO/NO_2	0.333	0.331	0.312	0.324	0.597

Table 4. NO/NO_x for the Eight Computational Cases in Table 3, (a) 15 km, (b) 20 km, and (c) 30 km (Contd)

(c) 30 km

Ratio	Ambient	I	II	III	IV
NO/NO_x [a]	0.248	0.244	0.168	0.195	0.967
$NO/(NO+NO_2)$	0.345	0.339	0.260	0.283	0.981
NO/NO_2	0.528	0.513	0.352	0.395	0.525
	Ambient	V	VI	VII	VIII
NO/NO_x [a]	0.080	0.079	0.042	0.068	0.880
$NO/(NO+NO_2)$	0.167	0.164	0.107	0.149	0.952
NO/NO_2	0.200	0.195	0.120	0.175	19.920

[a] NO/NO_x is taken as $NO/(NO + NO_2 + NO_3 + HNO_3 + HNO_4 + 2N_2O_5)$.

Cases I and V in Tables 3 and 4 show the effects of the homogeneous gas phase reactions only; that is, no heterogeneous wall loss for any of the species ($f = 0$). The behavior of species in the sampling tube in these two cases is, for the most part, predictable. Due to the relatively short average residence time of the sampled core (0.76 sec at 15 and 20 km, and 1.14 sec at 30 km), only those reactions with time constants comparable to or less than the residence time have any appreciable effect. Consequently, the most dramatic change in the ambient composition is the rapid decrease of O atom concentration upon sampling, due to reaction 25 (see Table 1). The half-life of O in the sampling tube due to this reaction varies from 1.7×10^{-4} sec at 15 km to 0.024 sec at 30 km. The time scales of most of the other reactions listed in Table 1 are significantly greater.

At 15 km, where diffusional losses to the sampling tube wall are relatively unimportant, the ambient composition is not seriously altered under almost any set of assumptions regarding wall loss "f" values (see Table 3a), especially with respect to those species related to the oxides of nitrogen. This is also reflected in the fact that the NO/NO_x ratios in Table 4a remain relatively constant for the eight computational cases considered. At 20 km (Tables 3b and 4b), the potential effect of diffusional losses to the tube wall becomes evident, and at 30 km (Tables 3c and 4c) the effect can be quite severe. However, the relatively small sensitivity of the absolute extent of wall loss to species identity shows that the variation in diffusivity among species is clearly a second order effect. Also, as shown by Cases I and V ($f = 0$) in Tables 3a, 3b, 3c, the homogeneous gas phase chemistry in the sampling tube is generally incapable of appreciably altering the sampled composition from that in the ambient; the residence times are simply too short.

Of the species examined, NO_3 and Cl exhibit large increases in concentration as a result of the homogeneous gas phase chemistry. NO_3 is observed to increase appreciably in Tables 3a and 3b due to production from NO_2 oxidation by ozone (that is, reaction 6 in Table 1). However, NO_3 is also rapidly consumed by NO (that is, reaction 7 in Table 1). Thus the ratio,

$$\frac{k_6 [O_3] [NO_2]}{k_7 [NO] [NO]} \tag{27}$$

controls the behavior of NO_3 in the sampling tube due to homogeneous gas phase chemist y. In addition, as shown in Table 3c, the NO_3 concentration can be severely affected by heterogeneous wall loss, to the point where production by NO_2 oxidation is completely overwhelmed, such that NO_3 decreases monotonically with progress through the flow tube. In any case, the NO_3 behavior should not have any appreciable effect on the total NO_x analyses, due to its relatively low expected concentration.

The behavior of Cl is somewhat analogous to that of NO_3. As can be seen from Table 3a, in Case I the Cl concentration increases by about a factor of twelve, while for Case V it actually decreases by approximately two-thirds. From the legend of Table 3, the only difference between Cases I and II is the absolute values of the ambient concentrations assumed for NO and NO_2. Obviously, in Case I, Cl increases due to the reaction of ClO with NO (that is, reaction 4 in Table 1); while in Case V, Cl decreases due to the reaction of Cl with O_3 (that is, reaction 20 in Table 1). Thus, the primary result of whether Cl increases or decreases during passage in the sampling table depends on the ratio:

$$\frac{k_4 [NO] [ClO]}{k_{20} [Cl] [O_3]} . \tag{28}$$

At 20 km the effect is qualitativ ly the same as for 15 km. At 30 km, however, Cl decreases monotonically from the ambient for both Cases I and V. The primary difference at 30 km is that the heterogeneous wall loss becomes significant enough to overcome Cl production via reaction 4, for the NO concentrations assumed.

This sensitive behavior of Cl suggests an interesting experimental approach for either NO measurements or the assessment of heterogeneous wall loss rates. Accurate values of the rate constants and Cl measurements as a function of distance in a sampling tube (using resonance fluorescence, for example) could be used to determine either, knowing something about the other.

4.2.2 NO_x/HNO_x

As concluded in the preceding section, and as is evident upon comparison of the three different NO/NO_x ratios for Cases I and V with their respective ambient values (that is, the ratios determined from the ambient concentrations assumed at the mouth of the sampling tube) in Tables 4a, 4b, and 4c, the homogeneous gas phase chemistry in the sampling tube is incapable of appreciably altering the NO_x/HNO_x sample composition. Thus, the only manner in which the sampling tube can affect the sampled ambient composition is via heterogeneous interactions with the tube wall. If this is the case, then the most severe effects on sampled composition should occur at the highest altitudes where the radial diffusivities are greatest. Examination of the 30 km results presented in Table 4c, reveals that of the cases studied, only IV and VIII result in appreciable alteration of the three NO/NO_x ratios from the ambient. Reference to the legend in Table 4 reveals that in these cases NO is assumed not to be lost at the wall (that is, $f=0$), while all the other NO_x/HNO_x species are assigned $f=1$. As discussed in Section 4.1, this scenario is not totally unreasonable in view of what is known about the behavior of these species, and would explain significant relative enhancement of NO over all the other NO_x/HNO_x species, as compared to ambient values. However, in order for this behavior to be predominant in the sampling tube, the magnitude of its effect must increase with altitude, and this is at variance with the data.

In general, the AFGL stratospheric NO and NO_2 mixing ratios, determined by Gallagher et al,[19] seem to be slightly lower than some other experimental observations at high altitudes, and slightly greater at low altitudes. The fact that the absolute values are of the same order of magnitude as those determined by other researchers with different experimental techniques, indicates that severe wall losses of NO and NO_2 at high altitudes, as exemplified by Cases II and VI in Tables 3a, 3b, and 3c (that is, for $f=1$), are improbable. Also, the severe discrimination against NO_x in comparison to NO, as exemplified by Cases IV and VIII in Table 3c (30 km, $f=1$) for NO_x/HNO_x and $f=0$ for NO), seems to be just as improbable. However, a comparison of "averaged" 30 km values reveals that the AFGL results are roughly one-third of some of the other experimental results. Thus, if heterogeneous wall loss in the sampling tube was the sole course of this discrepancy, then an overall average value of $f=0.5$ wall loss (that is, Cases III and VII in Table 3c) would explain the results relatively well. If this assumption applied at 20 km, the sampled NO and NO_2 values would be 83 and 86 percent respectively, of the ambient values (that is, Cases III and VII in Table 3c), which would place them in approximate agreement with other experimental

19. Gallagher, C.C., Forsberg, C.A., and Pieri, R.V. (1983) Stratospheric N_2O, CF_2Cl_2, and $CFCl_3$ composition studies utilizing in situ cryogenic whole air sampling methods, J. Geophys. Res. 88:3798.

observations (assuming, of course, that the other observations have no inherent experimental bias with respect to sampled vs ambient values). The actual case, however, is that the AFGL 20 km data are approximately a factor of two to three times greater than other experimental values.

Thus, there seems to be no consistent pattern in the AFGL NO and NO_2 results that unequivocally implicate heterogeneous wall interactions as the primary factor contributing to experimental bias introduced by the sampling tube of the cryogenic whole air sampler. However, there remain some more speculative possibilities that seem to be consistent with both significant heterogeneous effects and the observed data. For example, there is the possibility that the lower altitude data, which are relatively free of wall effects, are, therefore, more accurate representations of ambient values. In this case, the higher altitude data might be significantly affected by wall loss, and thus be biased towards lower values. Gallagher et al[20] present some results of a more recent two-dimensional stratospheric model prediction (Sze et al[21]) that seem to suggest this behavior; that is, the model predicts higher NO and NO_2 values than the AFGL data at high altitudes. (However, it also predicts lower values than the AFGL data at low altitudes.) Of course, if this scenario had any validity, this would imply that other experimental measurements are, in effect, too low. However, this possibility is not totally inconceivable, given possible experimental biases inherent in the other techniques, and natural local and temporal variations of NO and NO_x mixing ratios; either or both of which can account for the lower values observed.

Another possibility that is, in a sense, the inverse of the preceding one, and which also seems consistent with the known data, focuses on the operational characteristics of the balloon-borne cryogenic whole air sampler. Essentially, all the cryogenic whole air samples were taken on the descent leg of the balloon flight in order to avoid contamination from outgassing of the balloon and gondola. However, this procedure exposes the sampling tube wall, at relatively low temperatures, to the highest ambient concentrations of NO and NO_2 at high altitude prior to collection of the samples. Exposure at high altitudes occurs for enough time at conditions of high radial flux, due both to high radial diffusivities and high ambient mixing ratios, to accumulate significant amounts of NO_x/HNO_x, and even NO, if the actual capture coefficients are appreciable. The descent of the balloon to lower altitudes creates an unsteady-state situation with respect to wall accumulation due to decreased

---

20. Gallagher, C.C., Forsberg, C.A., Pieri, R.V., and Faucher, G.A. (1983a) Oxides of Nitrogen Content of Whole Air Samples Obtained at Altitudes From 12 to 30 km, submitted for publication.

21. Sze, N.D., Ko, M.K.W., Livshits, M., Wang, W.C., and Ryan, P.B. (1982) A Research Program for Atmospheric Chemistry, Radiation and Dynamics, AFGL-TR-82-0207, AD A120407.

radial fluxes of NO_x/HNO_x from the gas phase as a result of both lower mixing ratios and lower radial diffusivities. For example, NO and NO_2 radial wall fluxes near the sampling tube mouth, estimated from Eq. (19) (that is, for f = 1) using ambient mixing ratios from Fabian et al,[15] at the three altitudes considered here are:

Altitude (km)	N(NO) (cm^{-2} sec^{-1})	N(NO_2) (cm^{-2} sec^{-1})
30	1.2×10^9	6.2×10^9
20	1.2×10^9	3.4×10^8
15	5.3×10^7	4.8×10^7

As the wall flux of these species from the gas phase decreases during descent, some of the accumulated NO_x/HNO_x will tend to evaporate due to the prevailing unsteady-state situation created, thereby producing a net flux of species into the sampled gas; that is, the tube walls effectively outgas. This effect would tend to increase the NO and NO_2 values over those in the ambient for all lower altitudes during the course of a particular flight until the wall accumulation has been significantly dissipated.

This hypothesis qualitatively explains some of the salient characteristics of the AFGL data. First of all, due to the expected low tube wall temperatures (see Section 4.3), the net effusion from the walls at lower altitudes would be relatively slow. This would tend to account for the small absolute differences between the NO and NO_2 mixing ratios determined by the AFGL measurements and those from other techniques. An examination of the AFGL data reveals that although the NO values exhibit a drop-off with decreasing altitude, the total NO + NO_2 results are remarkably constant as a function of altitude (Gallagher et al[20]). This may involve a conversion of NO to NO_2 in the condensed phase on the tube wall according to the well-known stoichiometry (for example, see Chilton[22]):

$$NO + NO_2 + H_2O \rightarrow 2HNO_2 \; . \qquad (24)$$

The nitrous acid, which is unstable in the gas phase, would then decompose upon desorption at a lower altitude according to Eq. (25):

$$3HNO_2 \rightarrow HNO_3 + 2NO + H_2O \; . \qquad (25)$$

22. Chilton, T.H. (1968) Strong Water. Nitric Acid: Sources, Methods of Manufacture, and Uses, MIT Press, Cambridge, Massachusetts.

The net effect of Eqs. (29) and (25) is:

$$HNO_2 + NO_2 \rightarrow HNO_3 + NO \tag{30}$$

or, reduction of NO_2 to NO on a one-for-one basis. Thus, although NO would decrease, the total NO + NO_2 would remain relatively constant, since NO_2 is produced at the expense of NO.

As a rough, order-of-magnitude estimate of such a process, assume that by whatever mechanism, the tube walls become saturated with NO_2 at 30 km due to pre-sampling exposure. Upon descent to 20 km, the unsteady-state situation created thereby, would produce a net flux into the gas phase of approximately $(6.2 \times 10^{9} - 3.4 \times 10^{8}) = 5.86 \times 10^{9}$ cm^{-2} sec^{-1}. For a tube wall surface area of 600 cm $\times$ (π 7.6 cm) = 1.43×10^{4} cm^{2}, the net molecular flow into the sampled gas would be 8.4×10^{13} molecules/sec. Using a mixing ratio of 3×10^{-10} at 20 km (Fabian et al[15]), and the number density and volumetric flowrate in the sampling tube, the total inflow of NO_2 under these conditions would be: $(3 \times 10^{-10})(1.8 \times 10^{18}$ cm$^{-3})(1.89 \times 10^{4}$ cm^{3}/sec) = 1×10^{13} molecules/sec. Of course, the estimated outgassing rate of 8.4×10^{13} molecules/sec will tend to decrease with time, its instantaneous value determined in a complex fashion by in-flight operating factors and tube wall exposure history, and it will not be constant over the entire sampling tube length as assumed, so this is only a very approximate value. Nevertheless, the obvious implication of this estimate is that the outgassing rate can be of the same order-of-magnitude as the sampled ambient rate, thereby lending some credence to this hypothesis.

This "outgassing" hypothesis may also be consistent with the AFGL cryosampler data on nitrous oxide (N_2O) and Fluorocarbons 11 and 12 (Gallagher et al[19]). These species are known to be stable and their mixing ratios decrease with altitude in the stratosphere. Thus, the expected effect of the tube wall, consistent with the preceding, would be qualitatively quite different. At high altitudes the total wall flux would tend to decrease with altitude, primarily due to lower ambient mixing ratios. Therefore, the sampling tube wall would experience increasing wall fluxes during descent, which effectively inhibit outgassing. Thus, for these inert species, the only possible role of the tube wall is as an adsorber or sink, which would tend to decrease sampled compositions from those in the ambient at high altitudes where radial diffusivities are large. Although this trend is evident in the data presented by Gallagher et al[19] for N_2O, and Fluorocarbons 11 and 12, when compared with some model profiles (that is, good agreement at lower altitudes with increasing short-fall at higher altitudes), it is by no means unequivocal since the data also show extremely good agreement with other model predictions (see Gallagher et al[19]).

Of course, there are both in-flight and laboratory procedures and experiments that can be utilized to investigate this hypothesis and its potential impact further: for example, sampling simulation experiments through a flow tube in the laboratory; in-flight operational changes such as intermittent thermal desorption of wall deposits and re-equilibration prior to sampling, and/or sampling at lower altitudes first for NO_x; and so on. However, the feasibility of carrying out any of these efforts must be evaluated within the context of current and projected activity of the sampling program.

In addition to the two preceding scenarios involving the possible effects of heterogeneous phenomena at the sampling tube walls on the total cryogenic sample composition, there are probably others that can be formulated as well that are in qualitative agreement with the known data. Without additional experimental evidence regarding the precise nature of the processes at the tube wall, however, these must remain conjectures only.

4.3 Effect of Tube Wall Temperature

In considering factors that could significantly change the magnitude of the rate constant values assumed, the possibility of radiative solar heating of the Benway sample tubing was examined. Although no temperature measurements of the sampling tubing were made directly,* both the air temperature and the external surface temperature of the TRIWAS unit (at a point midway between the top and bottom) were recorded. This surface temperature should be roughly equivalent to the sampling tube wall temperature. As shown in Table 5, the temperature differences between the surface and air were both positive (8° C maximum) and negative (-9° C, maximum). These differences in temperature should not be large enough to cause any serious increase (or decrease) in air sample temperature due to heat transfer through the wall of the sampling tubing. An estimate of the potential magnitude of this effect follows.

Assuming a constant tube wall temperature, T_w, an energy balance on the sampled air is:

$$2\pi RL\, h\, \Delta T_{avg} = W\, C_p (T_2 - T_1) \qquad (31)$$

---

*Note added in proof: Since this report was written, a balloon flight package using the same sampling tube was fitted with thermistors placed at various locations and flown in the lower stratosphere. The maximum surface temperature throughout the 18-13 km sampling range was -17° C. Thus, clearly all the conclusions arrived at in this report are supported, and, indeed, may actually be conservative.

where

h	laminar flow wall heat transfer coefficient, cal/cm^2·sec·K,
ΔT_{avg}	= logarithmic mean temperature difference between the tube wall and average bulk temperature at the inlet and the sampling point,
W	air mass flow rate, g/sec,
C_p	specific heat capacity of the air, cal/g·K,
T_2	bulk temperature at sampling point,
T_1	bulk temperature at inlet.

The Nusselt number ($2hR/k_c$; k_c = thermal conductivity of air) for laminar tube flow with constant wall temperature is well known (for example, see Bird et al[5], p. 406). For the three sampling altitudes considered here and the flow conditions in Section 2.1:

Altitude (km)	ρ (g/cm^3)	W (g/sec)	Nu* -	h (cal/cm^2·sec)
15	1.95×10^{-4}	3.68	5.5	3.58×10^{-5}
20	8.67×10^{-5}	1.64	4.5	2.93×10^{-5}
30	1.78×10^{-5}	0.224	3.8	2.47×10^{-5}

Table 5. Typical Sampler Air Temperature Data

Time		Altitude (ft)	Sampler Temperature (°C)	Air Temperature (°C)	$\Delta T = T_s - T_a$) (°C)
5/31/81	1042 (LDT)	65,700	-29	-31	+2
	1310	47,500	-49	-45	-4
	1410	38,800	-43	-38	-5
6/4/81	1124	96,600	- 5	-10	+5
	1331	81,200	-11	-19	+8
	1526	64,600	-27	-29	+2
5/82	0950	66,620	-27	-27	0
	1233	49,380	-49	-40	-9
	1253	48,140	-46	-39	7

---

*Assuming k_c = 4.4 × 10^{-5} cal/cm·sec·K, and C_p = 6.973 cal/mol·K for air.)

Due to the relatively small temperature differences expected, ΔT_{avg} will be approximated as the arithmetic average. Substituting into Eq. (31) yields:

$$T_2 \cong \frac{\beta T_w + T_1 (1 - \beta/2)}{(1 + \beta/2)} \qquad (32)$$

where $\beta = \pi DLh'/WC_p$. Using the extreme values of the temperature differences presented in Table 5, together with the basic data from Section 2.1:

Altitude (km)	β	$(T_2 - T_1)$ (heated wall; max. +8K)	$(T_1 - T_2)$ (cooled wall; max. -9K)
15	0.020	0.15	-0.18
20	0.037	0.30	-0.33
30	0.026	1.62	-1.83

Another method of assessing the magnitude of the heat transfer effect is to estimate the tube wall temperature required to increase the air sample temperature by 10K:

Altitude (km)	Wall Temperature Required to Heat Air Sample 10K (K)	ΔT Above Ambient (K)
15	721.6 (448.5°C)	505.
20	492. (218.8°C)	275.4
30	280. (7.3°C)	49.2

Thus, even at 30 km,* there is no reason to suspect an air sample temperature increase (or decrease) even approaching 10K; that is, the 49.2K temperature difference required is significantly greater than the +8K or so suspected. The conclusion of this analysis is that the effect of temperature on processes within the sampling tube is completely negligible. In addition, since the tube wall temperatures are expected to be within 10K of ambient, heterogeneous interactions should also occur at approximately ambient temperatures.

5. SUMMARY AND CONCLUSIONS

A numerical model of a sampling tube used to conduct stratospheric air to the sampling point of a balloon-borne cryogenic whole air sampler, has been developed

---

*The effect of altitude is reflected by the ratio, β. Both the heat transfer coefficient, h, and the mass flow in the sampling tube, W, decrease with altitude; however, h decreases more slowly than W.

in order to assess the potential effects of passage through the tube on alteration of species mixing ratios from those in the ambient. This model is based on the application of a general purpose, homogeneous, multireaction chemical kinetics code (CHEMSEN) to a 31 reaction (49 reaction with heterogeneous wall loss), 23 species (42 species with adsorbed or "lost" constituents) stratospheric kinetic model, modified to take into account heterogeneous interactions with the tube wall. Essentially, the heterogeneous loss rates due to radial diffusion were transformed into equivalent pseudo-homogeneous reactions. This technique exploits the difference in time scales for radial diffusion and convection in the sampling tube. The resultant model represents a useful general tool for estimating the potential absolute and relative effects of the tube wall and homogeneous chemical reactions in altering the composition of complex flowing and reacting mixtures in atmospheric or laboratory applications.

The effects of the homogeneous gas phase chemistry and heterogeneous wall loss were estimated at three different altitudes: 15, 20, and 30 km. It was found that the gas phase chemistry was generally incapable of appreciably altering the sampled composition from that in the ambient. This result is primarily due to the short average residence time in the sampling tube. On the other hand, depending on the particular set of assumptions used, heterogeneous wall loss was found capable of imposing significant alterations on the sampled gas composition, particularly at altitudes above about 20 km, due to fast radial diffusion. The tube wall temperature was shown to have a completely negligible effect on the homogeneous gas phase kinetics.

Currently, definitive quantitative assessments of the impact of the heterogeneous interactions at the tube wall on the final sampled composition are hampered by lack of knowledge concerning the precise nature of the complex processes (of all those possible) that actually occur to a significant extent at stratospheric conditions and compositions. In this regard, the behavior of the tube wall with respect to any single species may range from that of a simple sink (of varying effectiveness, as reflected by the capture coefficient), to that of a complex chromatographic chemical reactor. However, two scenarios involving heterogeneous wall effects were suggested that at least qualitatively explain some trends observed in comparisons of various other data and model predictions with the AFGL cryosampler data. The "outgassing" hypothesis in particular, whereby NO_x species collected at high altitudes could be released at lower altitudes, seems deserving of further study.

In order to improve quantitative predictive techniques for the effects of sampling network walls on sampled compositions, good experimental data are needed to be used in conjunction with a practical numerical model. This report provides an approach and the rudiments of an appropriate model. However, the controlling heterogeneous physicochemical processes for species of interest at stratospheric

conditions remain to be unequivocally identified. Once this information is available, accurate parameter values can be experimentally determined for the model. In this regard, a chromatographic approach involving stimulus-response transient techniques is suggested and recommended.

References

1. Gallagher, C.C., and Pieri, R.V. (1976) Cryogenic Whole Air Sampler and Program for Stratospheric Composition Studies, AFGL-TR-76-0162.

2. Gallagher, C.C., Forsberg, C.A., Pieri, R.V., and Faucher, G.A. (1981) Stratospheric Trace Gas Composition Studies Utilizing In Situ Cryogenic, Whole-Air Sampling Methods, AFGL-TR-81-0071, AD A104375.

3. Sherman, C. (1983) private communication.

4. U.S. Standard Atmosphere (1976) NOAA, NASA, USAF, Washington, D.C.

5. Bird, R.B., Stewart, W.E., and Lightfoot, E.N. (1960) Transport Phenomena, Wiley & Sons, New York.

6. Taylor, G.I. (1953) Proc. R. Soc. A. 219A:186.

7. Taylor, G.I. (1954a) Proc. R. Soc. A. 223A:446.

8. Taylor, G.I. (1954b) Proc. R. Soc. A. 225A:473

9. Aris, R. (1956) On the dispersion of a solute in a fluid flowing through a tube, Proc. R. Soc. A. 235A:67.

10. Hunt, B. (1977) Int. J. Heat Mass Transfer 20: 393.

11. Crank, J. (1975) The Mathematics of Diffusion, Oxford University Press, London.

12. Kee, R.J., Miller, J.A., and Jefferson, T.H. (1980) CHEMKIN: A General-Purpose, Problem-Independent, Transportable, FORTRAN Chemical Kinetics Code Package, SAND 80-8003, Sandia National Laboratories, Livermore, California.

13. Kramer, M.A., Kee, R.J., and Rabitz, H. (1982) CHEMSEN: A Computer Code for Sensitivity Analysis of Elementary Chemical Reaction Models, SAND 82-8230, Sandia National Laboratories, Livermore, California.

14. The Stratosphere, 1981, Theory and Measurements (1982) WMO, NASA, FAA, NOAA, Report No. 11, NASA/Goddard Space Flight Center, Greenbelt, Maryland.

15. Fabian, P., Pyle, J.A., and Wells, R.J. (1982) Diurnal variations of minor constituents in the stratosphere modeled as a function of latitude and season, J. Geophys. Res. **87**:4981.

16. Greene, S.A., and Pust, H. (1958) Determination of nitrogen dioxide by gas-solid chromotography, Anal. Chem. **30**:1039.

17. Bentley, P.D., and Hands, B.A. (1978) Proc. Roy. Soc. (London) **A359**:319.

18. Calo, J.M., Fezza, R.J., and Dineen, E.J. (1981) Gas-Surface Interactions in Cryogenic Whole Air Sampling, AFGL-TR-81-0162, AD A108255.

19. Gallagher, C.C., Forsberg, C.A., and Pieri, R.V. (1983) Stratospheric N_2O, CF_2Cl_2, and $CFCl_3$ composition studies utilizing in situ cryogenics whole air sampling methods, J. Geophys. Res. **88**:3798.

20. Gallagher, C.C., Forsberg, C.A., Pieri, R.V., and Faucher, G.A. (1983a) Oxides of Nitrogen Content of Whole Air Samples Obtained at Altitudes From 12 to 30 km, submitted for publication.

21. Sze, N.D., Ko, M.K.W., Livshits, M., Wang, W.C., and Ryan, P.B. (1982) A Research Program for Atmospheric Chemistry, Radiation and Dynamics, AFGL-TR-82-0207, AD A120407.

22. Chilton, T.H. (1968) Strong Water. Nitric Acid: Sources, Methods of Manufacture, and Uses, MIT Press, Cambridge, Massachusetts.

Appendix A

Newton's Method Solution for α_1 [Eq. (23)]

Application of Newton's method to find the roots of Eq. (23) can be expressed as:

$$\alpha_1^{(i+1)} = \alpha_1^{(i)} - g(\alpha_1^{(i)})/g'(\alpha_1^{(i)}) \qquad \text{(A1)}$$

where (i) represents the current estimate for α_1, $g(\alpha_1^{(i)})$ is the value of the function,

$$g(\alpha_1^{(i)}) = \frac{f^2 D (1.25)^2}{R^2 J_1^{\,2}(\alpha_1^{(i)1/2} D^{-1/2} R)} - \alpha_1^{(i)} \qquad \text{(A2)}$$

and $g'(\alpha_1^{(i)})$ is the derivative of $g(\alpha_1^{(i)})$,

$$g'(\alpha_1^{(i)}) = -f^2 (1.25)^2 D \;\frac{\left[\alpha_1^{(i)1/2} D^{-1/2} R J_0 - J_1/\alpha\right]}{R^2 J_1^{\,3}} \qquad \text{(A3)}$$

wherein the arguments of all the Bessel functions are $(\alpha_1^{(i)1/2} D^{-1/2} R)$.

Iterative application of Eq. (A1) to convergence, using some predetermined criterion, will yield the value of α_1 for the parameters f, d, and R.

Appendix B

Subroutine KPRIME

```
SUBROUTINE KPRIME        74/74   OPT=1                        FTN 4.8+528

                SUBROUTINE KPRIME (AA,BB,EE,WT)
                REAL MMBSJ1,MMBSJ0
                DATA EPSI/1.0E-4/
                DATA T,P/0.0,0.0/
          C
                TEST=SIGN(1.0,AA)
                IF(TEST .GE. 0.0) RETURN
          C
                IF (BB .NE. 0.) T=BB
                IF (EE .NE. 0.) P=EE
                IF (T .NE. 0. .AND. P .NE. 0.) GO TO 10
                PRINT *,"T=   ",T,"   P=   ",P
                STOP1
          10    F=ABS(AA)
                D1=2.29*(40./(760.*P))*((T/220.)**1.5)
                D2=(1./29.)+(1./WT)
                D3=(1./29.)+(1./30.)
                D=D1*(D2**0.5/D3**0.5)
          C
                IF (F .LT. 1.) GO TO 20
                PRIMK=((2.4**2.)*D)/(3.8**2.)
                GO TO 999
          C
          20    IF (F .GT. 0.) GO TO 30
                PRIMK=0.
                GO TO 999
          C
          30    IF (F .GT. 0. .AND. F .LT. 1.) GO TO 40
                PRINT *,"F=   ",F
                STOP2
          40    CONST=(1.25/3.8)**2.
                AOLD=((2.4**2.)*D)/(3.8**2.)
                IPASS=0
          C
          201   ARG=(AOLD**0.5)*(D**(-0.5))*3.8
                IPASS=IPASS+1
                BES1=MMBSJ1(ARG,IER)
                BES0=MMBSJ0(ARG,IER)
                TOP=(F**2.)*CONST*D
                BOT=BES1**2.
                G=(TOP/BOT)-AOLD
                X1=(-(F**2.)*CONST*D)/(BES1**3.)
                X2=(AOLD**(-0.5))*(D**(-0.5))*3.8*BES0
                X3=X1*(X2-(BES1/AOLD))
                GP=X3-1.0
                ANEW=AOLD-(G/GP)
                DELTA=ABS(AOLD-ANEW)
          C
                IF (DELTA .LT. EPSI) GO TO 299
                AOLD=ANEW
                GO TO 201
          299   PRIMK=ANEW
          C
          999   AA=PRIMK
                BB=EE=0.0
                PRINT 100,WT,AA,BB,EE
          C
```


PRECEDING PAGE BLANK-NOT FILMED

84